치의과학석사 학위논문

Ginger and its two active components induce autophagy and apoptosis through C/EBP Homologous protein in oral squamous cell carcinoma

구강 편평상피세포암종에서 C/EBP Homologous protein을 통한 자가포식과 세포사멸을 유도하는 생강추출물 및 생리활성물질의 항암 효능에 관한 연구

2022 년 8 월

서울대학교 대학원

치의과학과 구강병리학전공

김 현 지

Ginger and its two active components induce autophagy and apoptosis through C/EBP Homologous protein in oral squamous cell carcinoma

구강 편평상피세포암종에서 C/EBP Homologous protein을 통한 자가포식과 세포사멸을 유도하는 생강추출물 및 생리활성물질의 항암 효능에 관한 연구

지도 교수 조 성 대

이 논문을 치의과학 석사학위논문으로 제출함

2022 년 6 월

서울대학교 대학원

치의과학과 구강병리학 전공

김 현 지

김현지의 석사 학위논문을 인준함

2022 년 7 월

위 원 장 _____ 홍 성 두 _____ (인)

부위원장 _____ 조 성 대 _____ (인)

위 원 _____ 이 재 일 _____ (인)

Abstract

Ginger and its two active components induce autophagy and apoptosis through C/EBP Homologous protein in oral squamous cell carcinoma

Hyun-Ji Kim

Program in Oral Pathology

Department of Dental science

Graduate school

Seoul National University

(Supervised by Professor Sung-Dae, CHO, D.V.M., Ph. D.)

Background: Rhizomes of *Zingiber officinale* (*Z. officinale*) display anti-oxidant, anti-inflammatory, anti-ulcer, and anti-tumor properties. I examined the effects of an ethanol extract of *Z. officinale* rhizomes (ZOE) against human oral squamous cell

carcinoma (OSCC) *in vitro* and identified the components responsible for its pharmacological activity.

Methods: I performed a Cell Counting Kit-8, soft agar, and trypan blue exclusion assays to examine the growth inhibitory effect of ZOE in human OSCC cell lines. ZOE-induced apoptosis in human OSCC cell lines was determined by DAPI staining, measurement of the sub-G_1 population, annexin V/PI double staining, and western blot analysis. I measured the effect of ZOE on autophagy and autophagic flux by microscopic analysis. High-performance liquid chromatography (HPLC) analysis was used to identify the active components of ZOE.

Results: ZOE exhibited an anti-proliferative effect on human OSCC cells and induced apoptosis as evidenced by increased cleaved PARP levels and apoptotic cells by fluorescence staining and flow cytometric analysis. ZOE treatment also induced LC3-II conversion, increased formation of autophagosomes or autolysosomes, and accumulation of endogenous LC3 puncta. However, ZOE disrupted autophagic flux by blocking lysosomal acidification, which was similar to that of chloroquine, a late autophagy inhibitor. Furthermore, ZOE simultaneously induced autophagy initiation and apoptosis induction

through the accumulation of C/EBP homologous protein (CHOP), an endoplasmic reticulum (ER) stress marker protein. An HPLC analysis of ZOE revealed that 1-dehydro-6-gingerdione and 8-shogaol were the active components, which were sufficient to induce autophagy initiation and apoptosis induction by enhancing CHOP expression.

Conclusion: The results suggest that ZOE and its two active components target CHOP, initiate autophagy and apoptosis, and may be useful therapeutics against human OSCC.

Keywords: *Zingiber officinale*; Autophagy; Apoptosis; Oral squamous cell carcinoma; 1-dehydro-6-gingerdione; 8-shogaol

Table of Contents

1. Introduction

Natural products have emerged as an alternative therapeutic strategy to conventional therapies because of reduced side effects and potentiated efficacies (Chamberlin et al, 2019). Ginger (the rhizomes of *Zingiber officinale* Roscoe), which is extensively consumed worldwide as a spice for food, has been used as a traditional remedy for digestive disorders including dyspepsia, nausea, gastritis, and diarrhea (Nikkhah Bodagh et al, 2019). It possesses anti-oxidant, anti-inflammatory, anti-ulcer, and anti-tumor properties by virtue of its complexity of bioactive components, which include gingerol, shogaol, zingiberene, paradol, and zingerone (Rahmani, 2014). Over the past few decades, many studies have examined the therapeutic potential of ginger extract and its components to treat various diseases including cancer. A number of studies suggest that ginger extract inhibits the growth of various cancers including colon (Abdullah et al, 2010), breast (Elkady et al, 2012), and cervical (Ansari et al, 2016) cancer. Among the active components of ginger extract, 6-gingerol, which is the most abundant component of ginger, and 6-shogaol, which is the

dehydrated form of gingerol in dried ginger, exhibit powerful anti-cancer activity (Mansingh et al, 2018, Radhakrishnan et al, 2014, Ling et al, 2010, Saha et al, 2014). However, the effects of ginger extract and its active components in human OSCC remain unknown.

Avoiding cell death is a cancer hallmark that enables tumor cells to proliferate continuously (Fernald and Kurokawa, 2013). Apoptosis or type I programmed cell death represents the intrinsic self-destruction mechanism to control tissue homeostasis and is a major pathway activated by chemotherapeutic drugs (Bai and Wang, 2014). Macroautophagy (referred to as autophagy) is an evolutionarily conserved and strictly regulated eukaryotic lysosomal degradation pathway in which excessive or defective intracellular components are sequestered and degraded in double-membraned autophagosomes and autolysosomes, respectively (Glick et al, 2010). Because autophagy is required for the maintenance of cellular homeostasis, autophagy deficiency is associated with a wide range of human diseases including neurodegenerative diseases and cancers (Yang and Klionsky, 2020). Excessive or persistent autophagy may induce autophagy-related cell death (type II programmed cell death)

independent or in conjunction with apoptosis under certain conditions (Yonekawa and Thorburn, 2013). Thus, the induction of autophagy and/or apoptosis following treatment with chemotherapy may be important for triggering cytotoxicity in cancer cells.

In this study, I evaluated the pharmacological effects of ethanol extract of *Z. officinale* rhizomes (ZOE) with respect to the induction of cellular events, such as autophagy initiation and apoptosis in human OSCC *in vitro*, which is attributed to the accumulation of CHOP protein. I also discovered that 1-dehydro-6-gingerdione and 8-shogaol, the active components of ZOE, play an important role as autophagy initiation and/or apoptosis inducers during OSCC therapy.

2. Materials & Methods

2.1. Preparation of *Z. officinale*

The rhizomes of *Z. officinale* Roscoe (ZO) were purchased from Gwang Myeong Dang Pharm Co., Ltd. (Ulsan, Republic of Korea) in April 2019 and identified by Prof. Se-Chan Kang (Kyung Hee University, Republic of Korea). A voucher specimen (KHU-BMRI-201904) has been stored at the Bio-Medical Research Institute, Kyung Hee University.

2.2. Isolation of the active components from ZO rhizomes

Dried ZO rhizomes (20.0 kg) were extracted with 70% aqueous ethanol (90 L × 4) at room temperature (RT) for 24 h. After filtration and concentration, the resulting concentrated ethanol extract (ZOE, 1.6 kg) was added to water (4.0 L) and successively partitioned with n-hexane (4.0 L × 3). Each layer was concentrated under reduced pressure to obtain the n-hexane (ZOH, 539 g), water (ZOW, 1061 g), and residue (ZOHR, 326 g) fractions. The ZOHR (326 g) fraction was subjected to SiO_2 column chromatography (c.c.,

Φ 7.0 × 16.0 cm) and eluted with n-hexane-EtOAc (4:1 → 1:1, 500 ml of each) to $CHCl_3$-MeOH-H_2O (30:3:1, 500 ml of each) while monitoring by TLC. This procedure yielded 14 fractions (ZOHR-1 to ZOHR-14). ZOHR-2 (46.3 g, Ve/Vt 0.125-0.250) was subjected to ODS c.c. (Φ 13 × 6 cm, acetone-water = 1:1, 8 L), which yielded 11 fractions (ZOHR-2-1 to ZOHR-2-11). ZOHR-2-6 (4.7 g, Ve/Vt 0.430-0.470) was subjected to SiO_2 c.c. (Φ 2 × 15 cm, CHCl3-EtOAc = 50:1 → 30:1 → 10:1, 2.7 L of each) to yield 16 fractions (ZOHR-2-6-1 to ZOHR-2-6-16) along with purified 1-dehydro-6-gingerdione (ZOHR-2-6-9, 100.8 mg, Ve/Vt 0.517-0.535, TLC [SiO_2] Rf 0.58, n-hexane-EtOAc = 3:1, TLC [ODS] Rf 0.51, acetone-MeOH-water = 4:1:1). ZOHR-2-8 (2.5 g, Ve/Vt 0.510-0.580) was subjected to SiO_2 c.c. (Φ 4.5 × 21 cm, n-hexane-EtOAc = 8:1, 7.5 L) to yield 11 fractions (ZOHR-2-8-1 to ZOHR-2-8-11). ZOHR-2-8-6 (446.0 mg, Ve/Vt 0.483-0.536) was subjected to ODS c.c. (Φ 3 × 7 cm, acetone-MeOH = 3:2, 2.4 L) to yield nine fractions (ZOHR-2-8-6-1 to ZOHR-2-8-6-9) along with purified 8-shogaol (ZOHR-2-8-6-6, 128.6 mg, Ve/Vt 0.675-0.775, TLC [SiO_2] Rf 0.61, n-hexane-EtOAc = 3:1, TLC

[ODS] Rf 0.78, acetone-water = 3:1). The structures of the isolated metabolites were verified by spectroscopic methods including NMR, IR, UV, and MS and by comparison of the data with existing data (Lee et al, 2011).

1-Dehydro-6-gingerdione (Metabolite No. 5): Yellow oil ($CHCl_3$); $C_{17}H_{22}O_4$; EI-MS m/z 290 [M]; 1H-NMR (600 MHz, $CDCl_3$, δH) 0.90 (3H, t, J = 6.8 Hz), 1.33 (4H, m), 1.61 (2H, m), 2.39 (2H, t, J = 7.8 Hz), 3.89 (3H, s), 5.63 (1H, s), 6.35 (1H, d, J = 15.6 Hz), 6.91 (1H, d, J = 8.4 Hz), 7.02 (1H, d, J = 1.8 Hz), 7.08 (1H, dd, J = 8.4, 1.8 Hz), 7.52 (1H, d, J = 15.6 Hz); 13C-NMR (150 MHz, CDCl3, δC) 200.19, 178.03, 147.64, 146.76, 139.81, 127.70, 122.59, 120.54, 114.79, 109.44, 100.12, 55.91, 40.08, 31.45, 25.30, 22.43, 13.91.

8-Shogaol (Metabolite No. 6): Yellow oil ($CHCl_3$); $C_{19}H_{28}O_3$; EI-MS m/z 304 [M]; 1H-NMR (600 MHz, $CDCl_3$, δH) 0.87 (3H, t, J = 7.2 Hz), 1.30-1.43 (10H, overlapped), 2.20 (2H, m), 2.79 (2H, overlapped), 2.86 (2H, overlapped), 3.86 (3H, s), 6.10 (1H, br.d, J = 16.0 Hz), 6.68 (1H, dd, J = 7.8, 1.8 Hz), 6.71 (1H, d, J = 1.8 Hz), 6.82 (1H, d, J = 7.8 Hz), 6.84 (1H, dt, J = 16.0, 7.2 Hz); 13C-NMR

(150 MHz, CDCl3, δC) 199.85, 147.91, 146.35, 143.79, 133.05, 130.16, 120.65, 114.28, 111.05, 55.71, 41.81, 32.36, 31.59, 29.75, 29.00, 28.91, 27.95, 22.49, 13.94.

2.3. Quantitative analysis of the active components of ZO rhizomes

Calibration curves for 1-dehydro-6-gingerdione and 8-shogaol were generated using five concentrations of each compound (3.125-50 μg/mL). ZOE was filtered through a 0.22 μm membrane filter (Woongki Science Co., Ltd., Seoul, Republic of Korea) and a 10 μl aliquot of each compound and ZOE was injected into the high-performance liquid chromatography (HPLC) system. HPLC analysis was done using a Waters 600S system (Waters, Milford, MA, USA) with a Waters 2487 UV detector (280 nm) and a Shim-pack GIST column (4.6 × 250 mm, particle size: 3 μm, Shimadzu, Kyoto, Japan). The mobile phase consisted of 0.1% FA in water (solvent A) and acetonitrile (solvent B), which were eluted at a flow rate of 0.4 ml/min with the following gradient elution: solvent B, 20% (0.01 min) → 30% (5 min) → 55% (10 min) → 55% (13 min) → 80% (25 min) → 80% (30 min) → 100% (60 min) → 100% (85 min). Quantitative

analysis was repeated three times. The regression curves and correlation coefficients (r^2) of 1-dehydro-6-gingerdione and 8-shogaol were y = 4476.7x-1445.9 (r^2 = 1.000) and y = 2906.6x-1784.9 (r^2 = 0.999), respectively. As a result, 1-dehydro-6-gingerdione and 8-shogaol were eluted at 54.37 and 50.89 min, respectively, and the amount in ZOE was determined to be 1.42 ± 0.10 and 0.13 ± 0.05 mg/g.

2.4. Cell culture and reagents

The human OSCC cell lines, HSC-2 and HSC-4 were kindly provided by Hokkaido University (Hokkaido, Japan). Both cell lines were cultured in DMEM/F-12 medium (WELGENE, Gyeongsan, Republic of Korea) supplemented with 10% fetal bovine serum (FBS) and 1% antibiotics (penicillin/streptomycin) in a humidified atmosphere containing 5% CO_2 at 37° C. All experiments were performed once the cells reached approximately 50% confluence. All chemicals, except 3-methyladenine (3-MA) and chloroquine (CQ), were dissolved in dimethyl sulfoxide (DMSO), aliquoted, and stored at -20° C until use, whereas 3-MA and CQ were dissolved in

distilled water (DW).

2.5. CCK-8 assay

Cells were seeded into 96-well plates and treated with the indicated concentrations of ZOE. After 24 h of treatment, 10 μl of CCK-8 solution (Dojindo Laboratories, Kumamoto, Japan) was added to each well and incubated at 37° C with 5% CO_2 for 1-2 h. Subsequently, the absorbance of each well was measured using a Chameleon microplate reader (Hidex, Turku, Finland) at 450 nm.

2.6. Soft agar assay

Basal Medium Eagle (BME, Sigma-Aldrich, St. Louis, MO, USA) was dissolved in DW with sodium bicarbonate to achieve a 2× BME solution and filtered through a 0.2 μm filter (Sartorius AG, Göttingen, Land Niedersachsen, Germany). A 1.25% agar was then prepared and mixed with 2× BME, L-glutamine, gentamicin, phosphate-buffered saline (PBS), and FBS to yield a 1.25% agar mix. Six-well plates were filled with 3 ml of 1.25% agar mix, including the indicated doses of ZOE per well, and allowed to solidify at RT for 1-2 h. A 2× BME

was then diluted in DW containing L-glutamine, gentamicin, and FBS to yield a 10% BME solution. Cells were prepared by suspending in 10% BME and mixing with agar. Thereafter, 1 ml of mixed cells was directly added onto the solidified bottom agar in six-well plates, allowed to solidify for 1-2 h at RT, and incubated in a humidified 37° C incubator with 5% CO_2 for approximately 4 weeks. To prevent the agar from drying out, six-well plates were covered with 200 μl of complete media diluted with the indicated doses of ZOE once a week. The colonies were imaged using a CKX53 microscope (Olympus, Tokyo, Japan) and counted with ImageJ software (National Institute of Health, Bethesda, MD, USA).

2.7. Western blot analysis

Whole protein lysates were prepared in 1× RIPA lysis buffer (Millipore Corp, Burlington, MA, USA) containing phosphatase inhibitor tablets (Thermo Scientific Inc., Rockford, IL, USA) and protease inhibitor cocktails (Roche, Mannheim, Germany). Protein concentrations were determined using a DC Protein Assay Kit (BIO-RAD Laboratories, Madison, WI, USA). Lysates containing equal

amounts of protein were separated by sodium dodecyl sulfate-polyacrylamide gel electrophoresis, electro-transferred to polyvinylidene difluoride membranes, and blocked with 5% skim milk in Tris-buffered saline containing Tween 20 (TBST) for 1 h at RT. The membranes were thoroughly washed with TBST and incubated overnight with the indicated primary antibodies at 4° C. Subsequently, the membranes were probed with horseradish peroxidase-conjugated secondary antibodies for 3 h at 4° C. The immunoreactive protein bands were detected using WestGlow™ FEMTO Chemiluminescent Substrate (BIOMAX, Seoul, Republic of Korea) on X-ray film or using the Image Quant LAS 500 system (GE Healthcare Life Sciences, Piscataway, NJ, USA). Supplementary Table 1 lists the primary and corresponding secondary antibodies for the target proteins.

2.8. Evaluation of nuclear morphological changes

After fixing with 70% ethanol at −20° C overnight, the cells were placed on a glass slide and stained with 2 μg/mL DAPI solution (Sigma-Aldrich, St. Louis, MO, USA) for 10 min. The morphological

changes of the apoptotic cells were assessed by fluorescence microscopy (Leica DMi8; Leica Microsystems GmbH, Wetzlar, Hesse, Germany).

2.9. Annexin V/PI double staining

Following treatment with the designated concentrations of chemicals, the cells were stained with an FITC Annexin V Apoptosis Detection Kit (BD Pharmingen, San Jose, CA, USA), following the manufacturer's instructions. The stained cells were dissected using an LSR Fortessa X-20 (BD Biosciences, San Jose, CA, USA), and the distribution of the cell populations was estimated with FlowJo software, version 9/10 (FlowJo LLC, Ashland, OR, USA).

2.10. Measurement of cell cycle distribution

Floating and adherent cells were collected and fixed with 70% ethanol overnight at −20° C. After washing with PBS, the fixed cells were stained with PI solution (20 μg/mL; Sigma, St. Louis, MO, USA) including RNase A (20 μg/mL; Thermo Scientific, Vilnius, Lithuania) for 15 min at 37℃. The cell cycle distribution was analyzed using a

FACSCalibur flow cytometer (BD Biosciences, San Jose, CA, USA), and the relative DNA distribution was reanalyzed by FlowJo software.

2.11. Transmission electron microscopy (TEM)

Following a 24-h treatment with either DMSO or ZOE, the cells were harvested and fixed with 2.5% glutaraldehyde in 0.1 M phosphate buffer for 24 h at 4° C. The fixed cell pellets were postfixed in 1% osmium tetroxide and embedded in Spurr low-viscosity resin. Thereafter, 1-μm-thick sections were arranged and stained with toluidine blue O. Uranyl acetate and lead citrate were also used to stain the sections. Morphological changes in the cells were observed under a JEM-1400 Flash Electron microscope (JEOL Ltd., Peabody, MA, USA) by the Electron Microscopy Core Facility in Seoul National University Hospital Biomedical Research Institute and by the Electron Microscopy Facility in Seoul National University Dental Research Institute.

2.12. Acridine orange (AO) staining

Cells were seeded in a four-well chamber slide with removable

wells (Thermo Scientific, Waltham, MA, USA) and incubated with or without ZOE at designated concentration for 24 h. ZOE-treated cells were then stained with 1 μg/mL AO (Invitrogen, Carlsbad, CA, USA) in a 37° C incubator for 15 min and then with 2 μg/mL DAPI solution at RT for 10 min. Subsequently, removable wells were detached and the stained cells were mounted with aqueous mounting medium without DAPI (Abcam, Cambridge, UK). Acidic vesicular organelles (AVO) were examined under LSM700 confocal laser scanning microscope (Carl Zeiss, Oberkochen, Baden-Württemberg, Germany).

2.13. Quantification of LC3 puncta

Both cell lines were cultured in a four-well chamber slide with removable wells and treated with the indicated concentrations of ZOE. After 24 h, the cells were fixed and permeabilized with Cytofix/Cytoperm solution (BD Biosciences, San Jose, CA, USA) for 1 h at 4° C and blocked with 0.1% BSA for 1 h at RT. Subsequently, the cells were incubated overnight at 4° C with primary antibody against LC3 followed by incubation with Alexa Fluor® 488-

conjugated secondary antibody for 3 h at RT. The formation of LC3 puncta was monitored under an LSM700 confocal laser scanning microscope with the appropriate filters.

2.14. Fluorescent tandem reporter assay for measuring autophagic activity

Cells were transfected with pDEST-CMV mCherry-GFP-LC3B WT plasmid (Addgene, Watertown, MA, USA) for 12 h using Lipofectamine 2000 transfection reagent according to the manufacturer's protocol. After transfection, the reduced serum medium was replaced with fresh complete medium, and the cells were maintained in complete medium containing G418 to select for the fluorescent tandem reporter-overexpressing cells. The established cells were seeded into a four-well chamber slide with removable wells and incubated with the indicated doses of ZOE for 24 h. Immunofluorescence analysis of cells expressing pDEST-CMV mCherry-GFP-LC3B WT plasmid was monitored with an LSM700 confocal laser scanning microscope using the appropriate filters.

2.15. Trypan blue exclusion assay

Cells were detached with 2× trypsin and diluted in PBS. Diluted cells were mixed with 0.4% trypan blue (Lonza, Walkersville, MD, USA) at a 1:1 ratio. The number of viable cells was determined using a CytoSMART automatic cell counter (Corning, Tewksbury, MA, USA).

2.16. Statistical analysis

All graphs were prepared using GraphPad Prism version 8.0 (GraphPad Software, San Diego, CA, USA), and all statistical analyses were done using SPSS version 26.0 (SPSS, Chicago, IL, USA). All data are presented as the mean ± standard deviation (SD) of three independent biological experiments. Statistical significance was estimated using either a two-tailed Student's t-test or one-way ANOVA with Tukey's post hoc test. A p-value < 0.05 was considered statistically significant (* or #).

3. Results & Figures

3.1. ZOE facilitates growth inhibition and apoptosis induction in human OSCC cell lines.

To determine the cytotoxic effects of ZOE in human OSCC *in vitro*, I conducted a CCK-8 assay using two OSCC cell lines (HSC-2 and HSC-4) exposed to the indicated doses of ZOE for 24 h. As shown in Fig. 1A, ZOE treatment significantly diminished the viability of both cell lines in a dose-dependent manner. Consistently, ZOE treatment suppressed the clonogenic growth of both cells as evidenced by reduction of the number and size of the colonies in soft agar plates (Fig. 1B). To verify whether the cytotoxic effect of ZOE was attributed to the induction of apoptotic signals in human OSCC cell lines, I measured the expression of cleaved PARP, which is considered a classical apoptosis marker. I found that ZOE treatment markedly increased the expression levels of cleaved PARP (Fig. 2A). These results were further supported by the enhanced levels of cleaved caspase-3 in ZOE-treated cells than in the control group

(Fig. 2B), which suggests that ZOE facilitates intracellular apoptotic events mediated by caspase activation in human OSCC cell lines. In addition, I determined the apoptotic effect of ZOE using fluorescence staining and flow cytometric analysis. Compared with the control groups, ZOE treatment markedly increased fragmented and condensed nuclei, which are considered typical morphological changes for apoptotic cells (Fig. 3A). I also observed that ZOE treatment apparently increased the number of apoptotic cells, as evidenced by increased populations within the sub-G_1 phases and annexin V-positive compartments (Fig. 3B and 3C). Overall, these data indicate that ZOE has a substantial growth inhibitory effect against human OSCC cells *in vitro*, which may result, in part, from the induction of apoptosis.

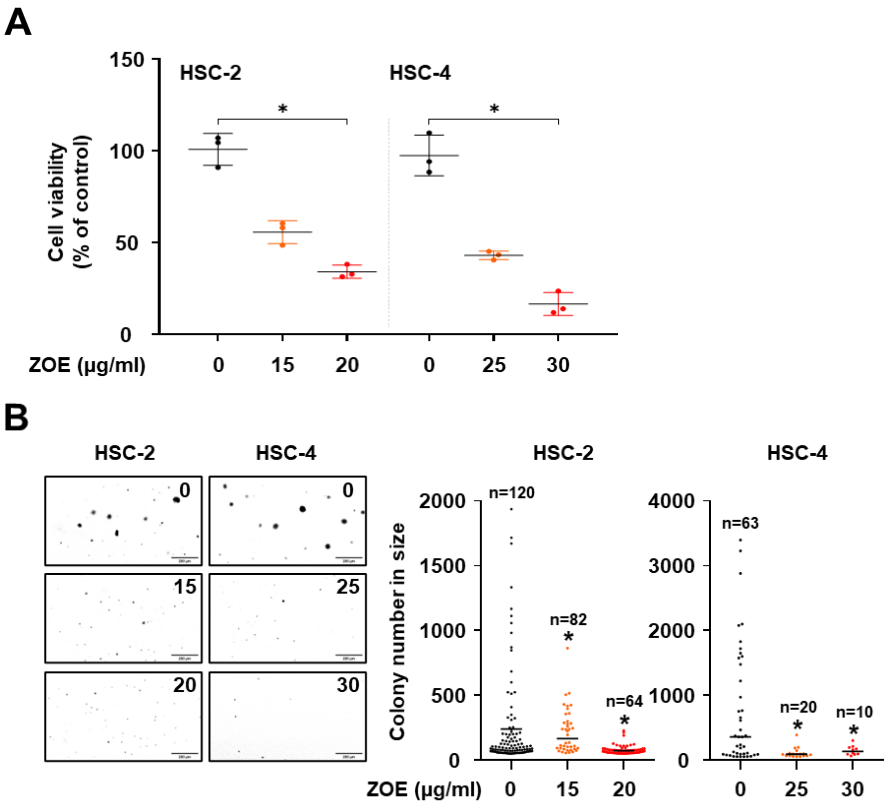

Fig. 1. The effect of ZOE on growth inhibition in human OSCC cell lines. HSC-2 and HSC-4 cells were treated with DMSO or the indicated concentrations of ZOE for 24 h (A) or once a week for 1 month (B). **(A)** Cell viability was assessed using a CCK-8 assay kit. **(B)** Representative images of the soft agar assay (left panel). Colonies were automatically counted using ImageJ software (right panel). Magnification, ×40; scale bar, 200 μm. All graphs are expressed as the mean ± SD of three independent experiments. *, $P < 0.05$ by one-way ANOVA.

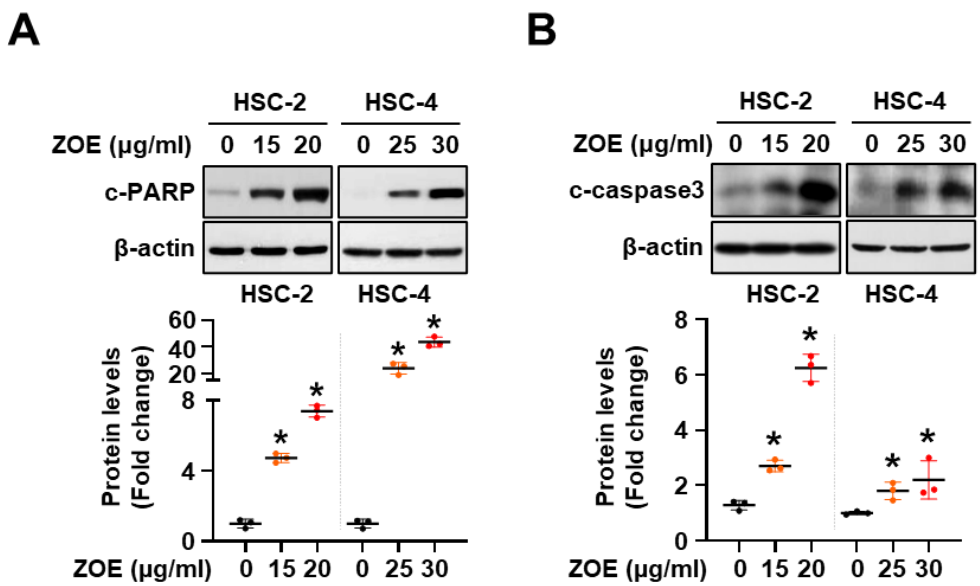

Fig. 2. The effect of ZOE on apoptosis related protein expression in human OSCC cell lines. HSC-2 and HSC-4 cells were treated with DMSO or the indicated concentrations of ZOE for 24 h. **(A)** Western blot images and graph showing the expression of cleaved PARP. β-actin was used as a loading control. **(B)** Western blot images and graph showing the expression levels of cleaved caspase-3. β-actin was used as a loading control. All graphs are expressed as the mean ± SD of three independent experiments. *, $P < 0.05$ by one-way ANOVA.

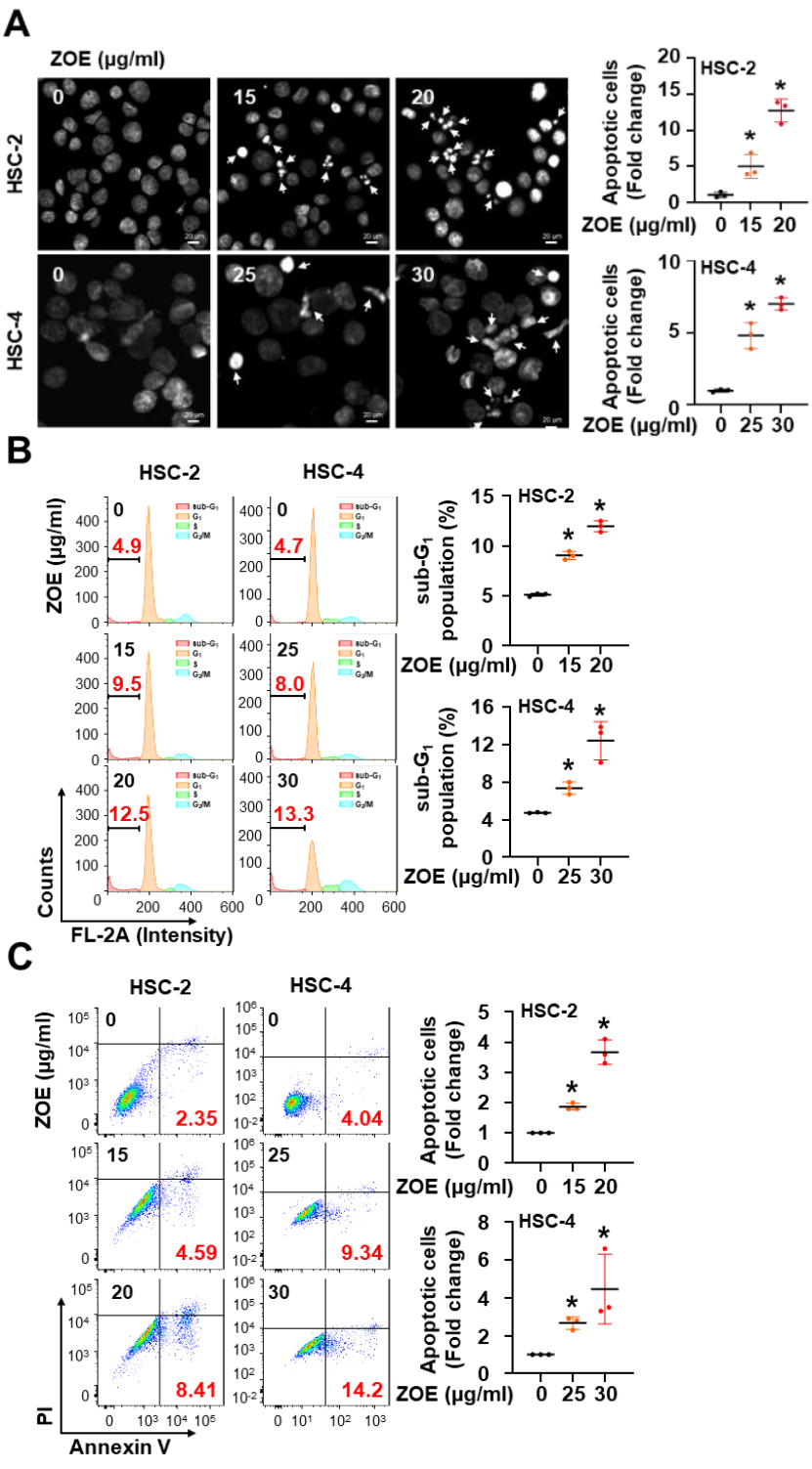
A
ZOE (μg/ml)
HSC-2
HSC-4
0
15
20
25
30
Apoptotic cells (Fold change)
ZOE (μg/ml) 0 15 20
ZOE (μg/ml) 0 25 30
B
HSC-2
HSC-4
ZOE (μg/ml)
4.9
4.7
9.5
8.0
12.5
13.3
sub-G1 population (%)
Counts
FL-2A (Intensity)
C
2.35
4.04
4.59
9.34
8.41
14.2
PI
Annexin V

Fig. 3. The effect of ZOE on apoptosis in human OSCC cell lines. HSC-2 and HSC-4 cell lines were treated with DMSO or the indicated doses of ZOE for 24 h. **(A)** Representative images of DAPI-stained HSC-2 and HSC-4 cells. Magnification, ×400; Scale bar, 20 μm. The white arrows indicate apoptotic cells. **(B and C)** Apoptosis was assessed using two FACS analyses, Sub-G1 population analysis and Annexin V / PI double staining. All results are expressed as mean ± SD of triplicate experiments. $*P < 0.05$ by one-way ANOVA.

3.2. ZOE promotes autophagy initiation in human OSCC cell lines

I examined ZOE-treated cells morphologically and observed the formation of peculiar vacuoles in the cytoplasm compared with control cells (Fig. 4A). Cytoplasmic vacuolization is a morphological characteristic of autophagy. To determine whether ZOE treatment regulates autophagy in human OSCC cell lines, I used western blot analysis to examine the conversion of LC3-I to LC3-II, which is a classical indicator for monitoring the formation of autophagosomes. As expected, ZOE treatment significantly increased lipidated LC3-II conversion and another autophagy marker, p62 (Fig. 4B). Subsequently, I verified the appearance of double-membrane autophagosomes or autolysosomes using TEM, the gold standard technique for autophagy identification. As shown in Fig. 5, the accumulation of double-membrane autophagosomes, which contain cytoplasmic materials, and autolysosomes was observed in ZOE-treated cells, but not in control cells. I then monitored the formation of AVO by AO staining, a method to detect autophagy. An abundance of AVO with red fluorescence in the cytoplasm was observed in ZOE-treated cells in a dose-dependent manner (Fig. 6A). In addition,

there was a significant accumulation of endogenous LC3 puncta in ZOE-treated cells (Fig. 6B). These data indicate that ZOE promotes autophagy in human OSCC cells *in vitro*, which may contribute to the growth inhibitory effect of ZOE.

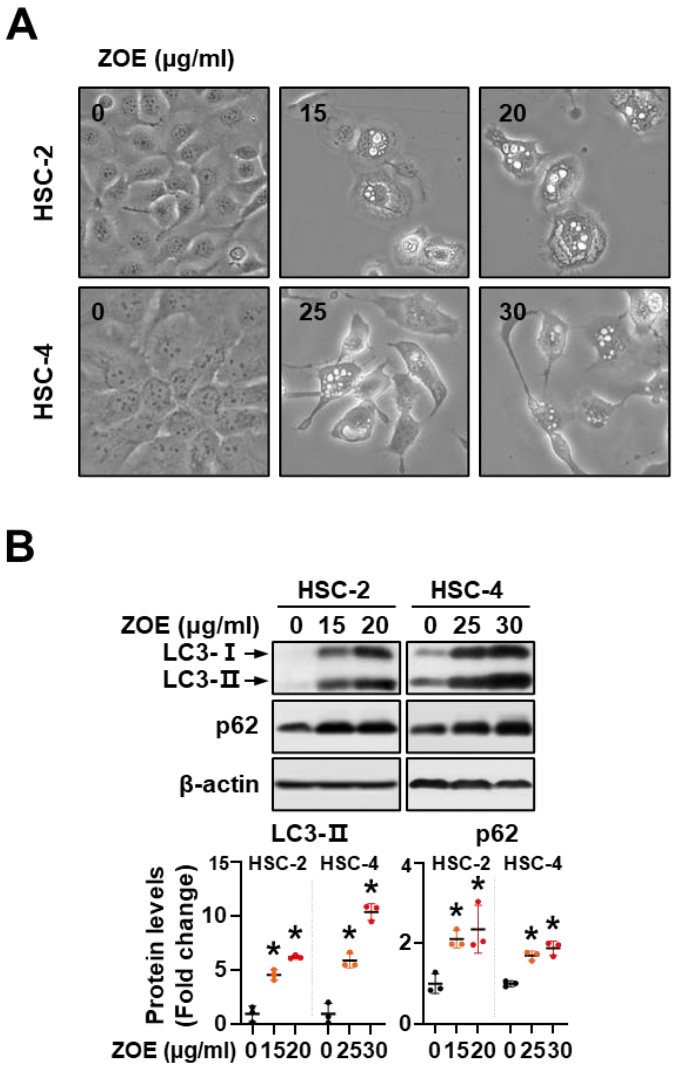

Fig. 4. The effect of ZOE on autophagy initiation in human OSCC cell lines. HSC-2 and HSC-4 cells were treated with DMSO or the indicated concentrations of ZOE for 24 h. **(A)** Representative images of phase-contrast microscopy in ZOE-treated cells. **(B)** Western blot images showing the expression levels of LC3-Ⅱ and p62. β-

actin was used as an internal control. All graphs represent the mean ± SD of three independent experiments. *, $P < 0.05$ by one-way ANOVA.

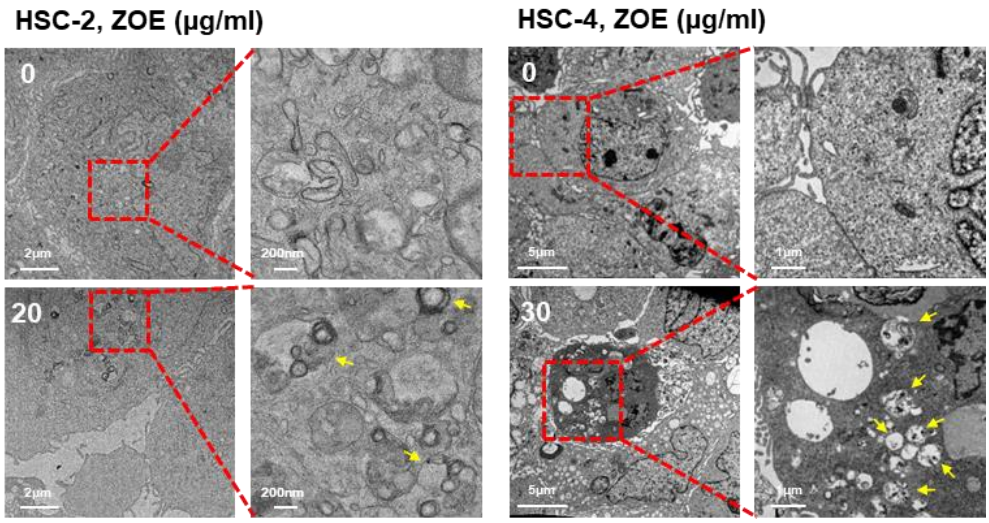

Fig. 5. The effect of ZOE on autophagy initiation in human OSCC cell lines. HSC-2 and HSC-4 cells were treated with DMSO or the indicated concentrations of ZOE for 24 h. Representative images of TEM. The red line boxed area was enlarged to the right. The yellow arrows indicate autophagosomes and autolysosomes. Magnification, ×3,000 or ×15,000 in HSC-2 and ×5,000 or ×20,000 in HSC-4; scale bar, 2 μm or 200 nm in HSC-2 and 5 μm or 1 μm in HSC-4.

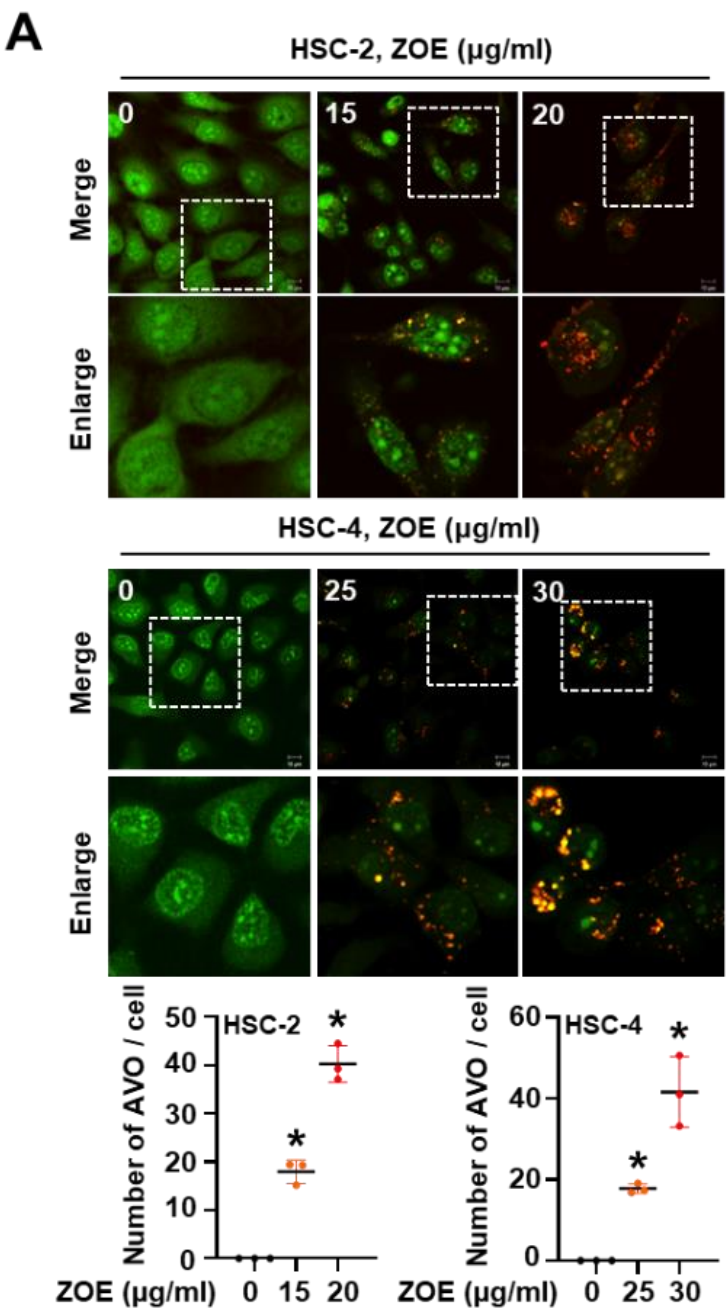
A
HSC-2, ZOE (μg/ml)
0
15
20
Merge
Enlarge
HSC-4, ZOE (μg/ml)
0
25
30
Merge
Enlarge
Number of AVO / cell
HSC-2
50
40
30
20
10
0
*
*
ZOE (μg/ml) 0 15 20
Number of AVO / cell
HSC-4
60
40
20
0
*
*
ZOE (μg/ml) 0 25 30

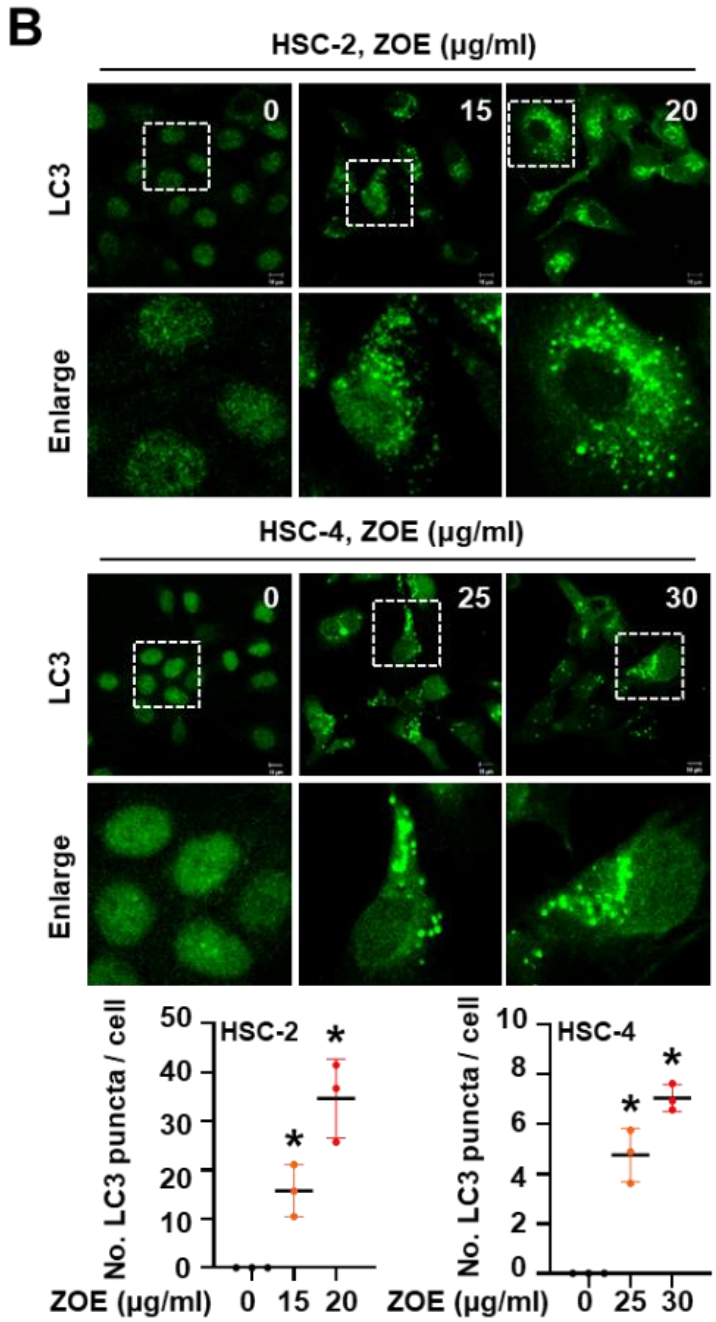
B
HSC-2, ZOE (μg/ml)
LC3
Enlarge
0
15
20
HSC-4, ZOE (μg/ml)
0
25
30
No. LC3 puncta / cell
HSC-2
ZOE (μg/ml) 0 15 20
HSC-4
ZOE (μg/ml) 0 25 30

Fig. 6. The effect of ZOE on autophagy initiation in human OSCC cell lines. HSC-2 and HSC-4 cells were treated with DMSO or the indicated concentrations of ZOE for 24 h. **(A)** Representative images of AVO stained with AO reagent. The white line boxed area was enlarged to the bottom. Magnification, ×400; scale bar, 10 μm. **(B)** Representative images of LC3 puncta formation. The white line boxed area was enlarged to the bottom. Magnification, ×400; scale bar, 10 μm. All graphs represent the mean ± SD of three independent experiments. *, $P < 0.05$ by one-way ANOVA.

3.3. ZOE blocks autophagic flux in human OSCC cell lines

Based on the above results, I found that ZOE promoted the expression of p62, an autophagy cargo protein that is transported to the autolysosomes for degradation. Because the accumulation of p62 protein implicates the inhibition of autophagy activity, I determined whether ZOE treatment impairs autophagy flux in human OSCC cell lines. Cells were pretreated with CQ, a late autophagy inhibitor, followed by ZOE treatment. As shown in Fig. 7A, both CQ and ZOE alone promoted LC3-II conversion. In addition, LC3-II accumulation induced by ZOE treatment was significantly enhanced by CQ cotreatment, suggesting that ZOE and CQ have an additive effect on autophagic flux inhibition. This was further supported by enhanced endogenous LC3 puncta accumulation following cotreatment of cells with CQ and ZOE compared with either compound alone (Fig. 7B). In contrast, ZOE-induced LC3-II accumulation was slightly decreased in both cell lines treated with 3-MA, an early autophagy inhibitor that blocks autophagosome formation (Fig. 7C). To confirm whether ZOE genuinely disturbed autophagic degradation, cells were stably

transfected with pDEST-CMV mCherry-GFP-LC3B WT plasmid, which shows a difference in pH stability between mCherry and GFP fluorescent proteins at acidic pH values. In the acidic condition of the autolysosome, acid pH-sensitive green fluorescence is quenched, whereas only red fluorescence appears as it is stable. However, when autophagy flux is impaired because of a disturbance in either autophagosome-lysosome fusion or lysosomal acidification, yellow puncta resulting from green and red fluorescence appear. As shown in Fig. 8, ZOE markedly increased yellow puncta without accumulation of red puncta, which indicates that ZOE and CQ disturb the maturation of autophagosome into autolysosomes and/or lysosomal acidification. However, I previously observed autolysosomes in ZOE-treated cells using TEM analysis, which suggests that ZOE does not inhibit the maturation of autophagosomes into autolysosomes. Therefore, these data suggest that ZOE impairs autophagic flux by blocking lysosomal acidification in human OSCC cell lines, which subsequently triggers the accumulation of autophagosomes.

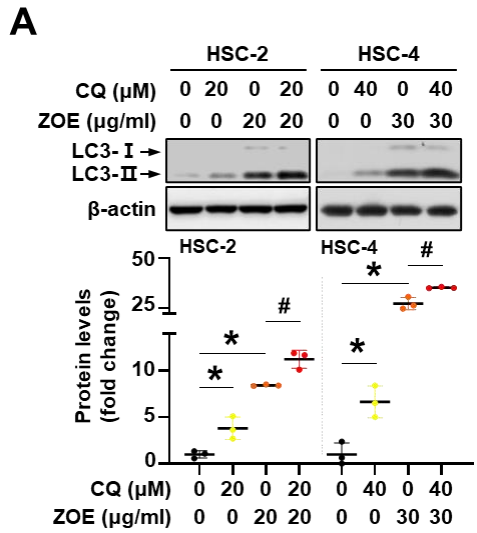
A
HSC-2
HSC-4
CQ (μM) 0 20 0 20 0 40 0 40
ZOE (μg/ml) 0 0 20 20 0 0 30 30
LC3- Ⅰ
LC3-Ⅱ
β-actin
HSC-2
HSC-4
Protein levels (fold change)
50
25
10
5
0
*
#

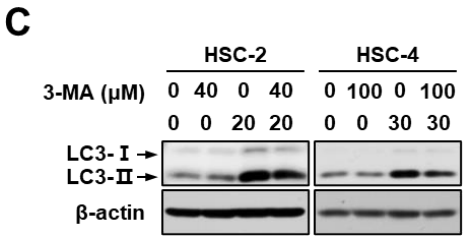
C
HSC-2
HSC-4
3-MA (μM) 0 40 0 40 0 100 0 100
0 0 20 20 0 0 30 30
LC3- Ⅰ
LC3-Ⅱ
β-actin

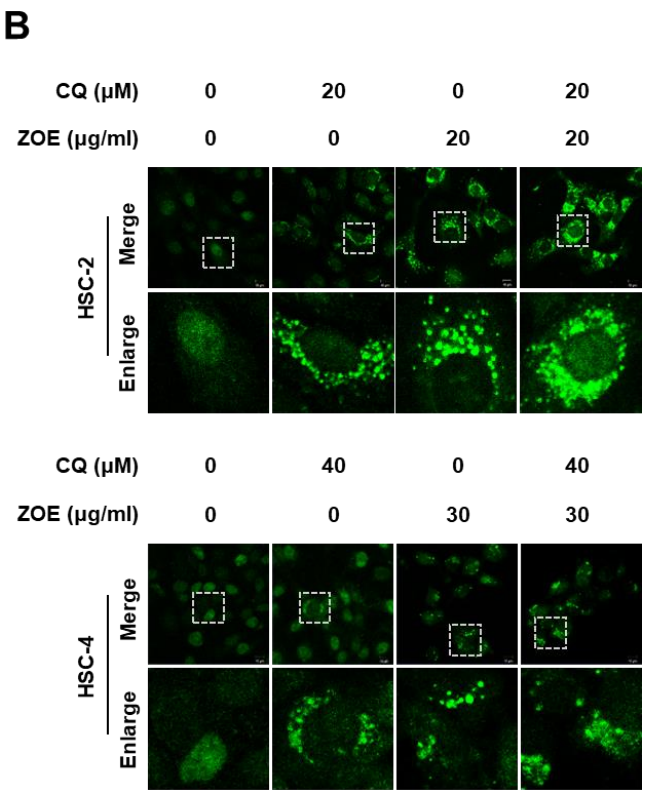
B
CQ (μM) 0 20 0 20
ZOE (μg/ml) 0 0 20 20
HSC-2
Merge
Enlarge
CQ (μM) 0 40 0 40
ZOE (μg/ml) 0 0 30 30
HSC-4
Merge
Enlarge

Fig. 7. The effect of ZOE on autophagic flux in human OSCC cells. HSC−2 and HSC−4 cells were pretreated with DW or the indicated concentrations of CQ or 3−MA for 2 h, followed by treatment with DMSO or the indicated concentrations of ZOE for 24 h (A and B) or 9 h (C). **(A and C)** Western blot images and graph showing the expression of LC3−II. β−actin was used as an internal control. **(B)** Representative images of LC3 puncta formation. The white line boxed area was enlarged to the bottom. Magnification, ×400; scale bar, 10 μm. All graphs indicate the mean ± SD of three independent experiments. * or #, $P < 0.05$ by one−way ANOVA.

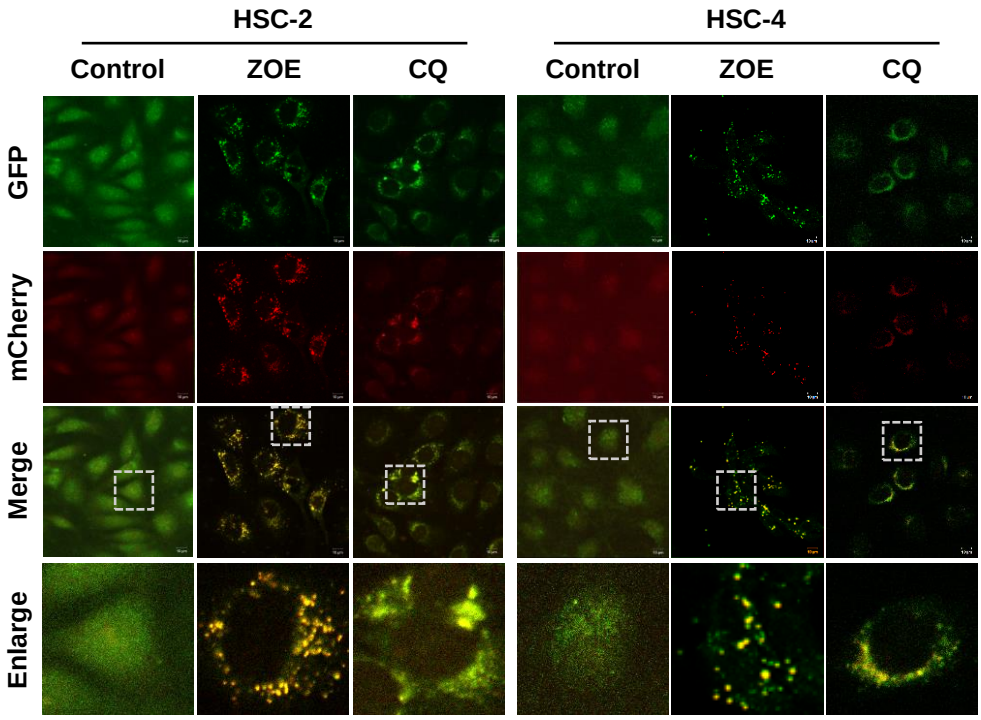
HSC-2
HSC-4
Control
ZOE
CQ
Control
ZOE
CQ
GFP
mCherry
Merge
Enlarge

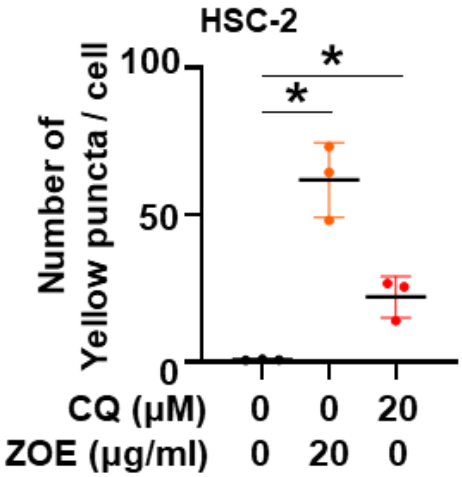
HSC-2
Number of Yellow puncta / cell
100
50
0
*
*
CQ (μM) 0 0 20
ZOE (μg/ml) 0 20 0

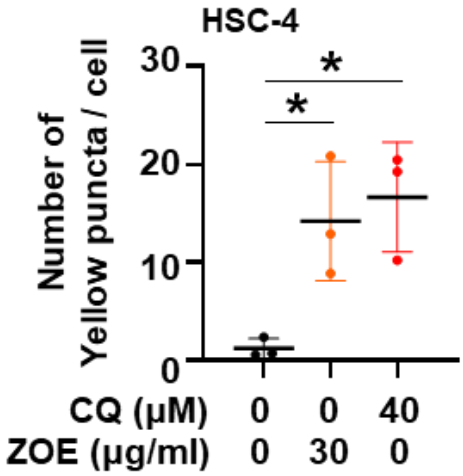
HSC-4
Number of Yellow puncta / cell
30
20
10
0
*
*
CQ (μM) 0 0 40
ZOE (μg/ml) 0 30 0

Fig. 8. The effect of ZOE on autophagic flux in human OSCC cells. HSC-2 and HSC-4 cells were treated with DMSO or the indicated concentrations of ZOE or CQ for 24 h. Representative images of immunofluorescence staining of cells expressing the pDEST-CMV mCherry-GFP-LC3B WT plasmid. Magnification, ×400; scale bar, 10 μm. All graphs indicate the mean ± SD of three independent experiments. *, $P < 0.05$ by one-way ANOVA.

3.4. ZOE simultaneously provokes autophagy initiation and apoptosis induction by enhancing CHOP expression

Endoplasmic reticulum (ER) stress plays a pivotal role in determining cell death by inducing autophagy and/or apoptosis-related signaling (Shi et al, 2016, Song et al, 2017, Zhou et al, 2017). To determine whether ZOE-induced cell death was caused by the induction of ER stress, I measured the expression of CHOP, which is commonly used as a marker of ER stress. The results indicated that ZOE treatment markedly augmented the expression levels of CHOP in a dose-dependent manner (Fig. 9A). I further examined the correlation between ER stress, autophagy, and apoptosis following ZOE treatment. Results showed that the expression levels of CHOP, LC3-II, and cleaved PARP significantly increased beginning 6 h after ZOE treatment (Fig. 9B and 9C). Therefore, these data indicate that ZOE promotes ER stress in human OSCC cell lines, which may simultaneously facilitate autophagy initiation and apoptosis induction.

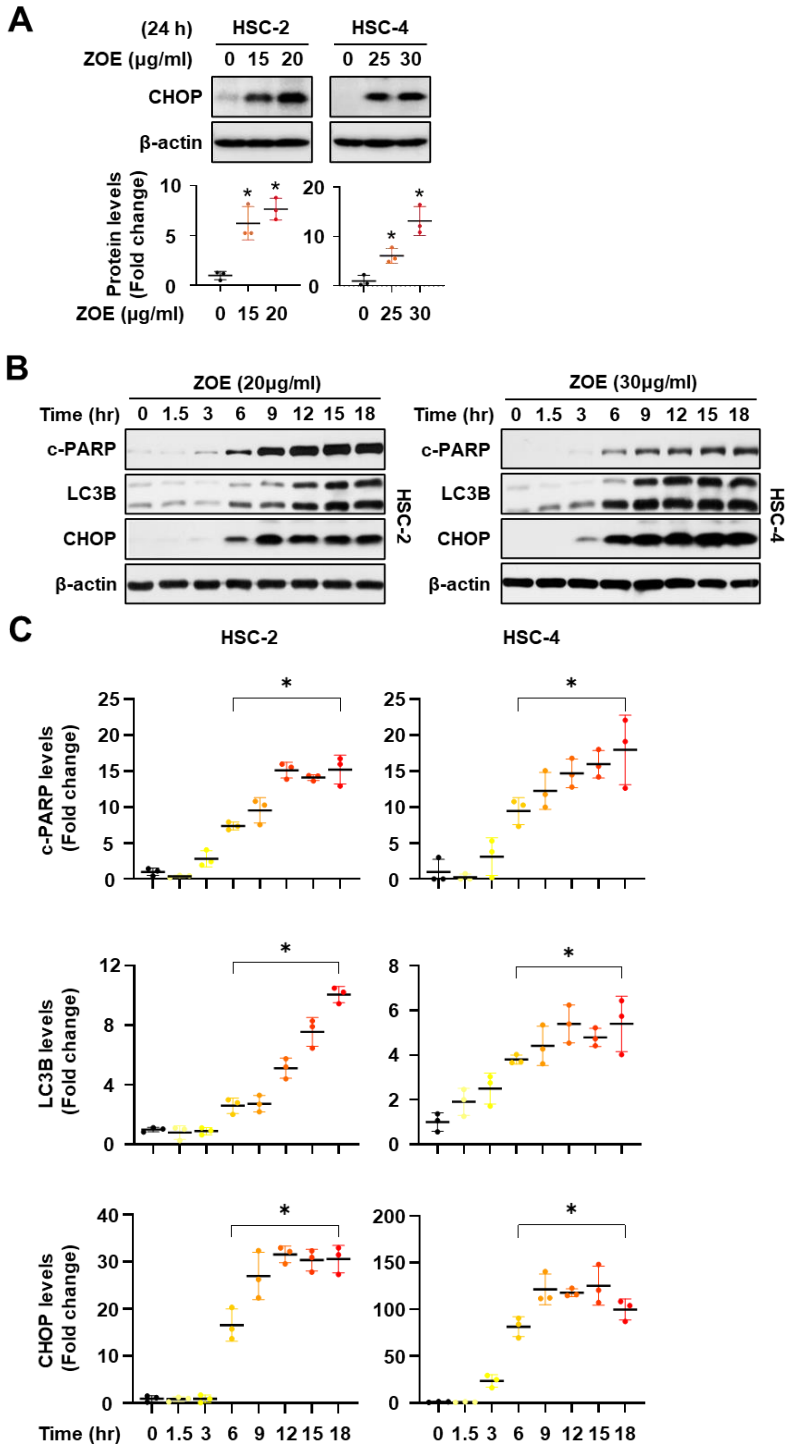
A
(24 h)
HSC-2
HSC-4
ZOE (μg/ml)
0 15 20
0 25 30
CHOP
β-actin
Protein levels (Fold change)
ZOE (μg/ml)
B
ZOE (20μg/ml)
ZOE (30μg/ml)
Time (hr)
0 1.5 3 6 9 12 15 18
c-PARP
LC3B
CHOP
β-actin
HSC-2
HSC-4
C
HSC-2
HSC-4
c-PARP levels (Fold change)
LC3B levels (Fold change)
CHOP levels (Fold change)
Time (hr)

Fig. 9. The relationship between ZOE-induced ER stress, autophagy, and apoptosis. HSC-2 and HSC-4 cells were treated with DMSO or the indicated concentrations of ZOE for each indicated time. **(A)** Western blot images and graphs showing the expression levels of CHOP. β-actin was used as a loading control. **(B)** Western blot images representing the expression levels of cleaved PARP, LC3-II, and CHOP at the indicated time points. β-actin was used as a loading control. **(C)** All graphs indicate the mean ± SD of three independent experiments. *, $P < 0.05$ by one-way ANOVA.

3.5. 1-Dehydro-6-gingerdione and 8-shogaol are the active components of ZOE that promote autophagy initiation and apoptosis induction via inducing CHOP expression

To identify which components of ZOE simultaneously induce autophagy initiation and apoptosis induction accompanied with CHOP enhancement in human OSCC cell lines, I carried out metabolite profiling of ZO rhizomes using quantitative HPLC analysis. As shown in Fig. 10A, I identified seven potent metabolites: 6-gingerol (1), 8-gingerol (2), 6-shogaol (3), 10-gingerol (4), 1-dehydro-6-gingerdione (5), 8-shogaol (6), and 8-paradol (7). To determine the effect of these metabolites on the growth of human OSCC cell lines, cells were treated with the same doses of metabolites. Of these metabolites, 6-shogaol (3), 1-dehydro-6-gingerdione (5), 8-shogaol (6), and 8-paradol (7) markedly inhibited the growth of both cell lines (Fig. 10B); however, only 1-dehydro-6-gingerdione (5) and 8-shogaol (6) consistently showed greater effects at enhancing CHOP, LC3-II, and cleaved PARP expression in both cell lines (Fig. 10C). Based on these results, I selected two metabolites, 1-

dehydro-6-gingerdione and 8-shogaol, for further mechanistic studies (Fig. 11A). To confirm whether the two metabolites represent authentic active components of ZOE and trigger the growth inhibitory effects in human OSCC cell lines, I performed a trypan blue exclusion assay. As shown in Fig. 11B, 1-dehydro-6-gingerdione and 8-shogaol dramatically suppressed the growth of human OSCC cell lines in a dose-dependent manner. Moreover, I found that 1-dehydro-6-gingerdione and 8-shogaol treatment resulted in dose-dependent increases of CHOP, LC3-II, and cleaved PARP in both cell lines (Fig. 12A). These findings were supported by increased populations within annexin V-positive compartments (Fig. 12B). Therefore, these data indicate that 1-dehydro-6-gingerdione and 8-shogaol are active components of ZOE, which simultaneously trigger autophagy initiation and apoptosis induction by inducing CHOP expression in human OSCC cells *in vitro*.

A

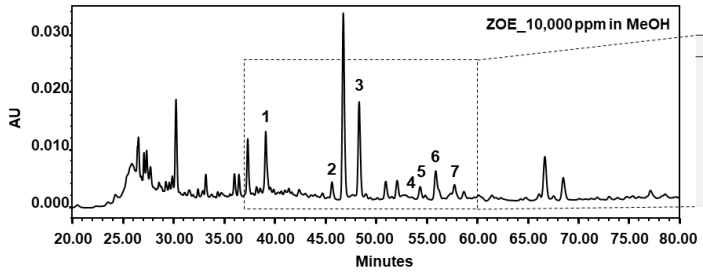

No.	Metabolites
1	6-gingerol
2	8-gingerol
3	6-shogaol
4	10-gingerol
5	1-dehydro-6-gingerdione
6	8-shogaol
7	8-paradol

B

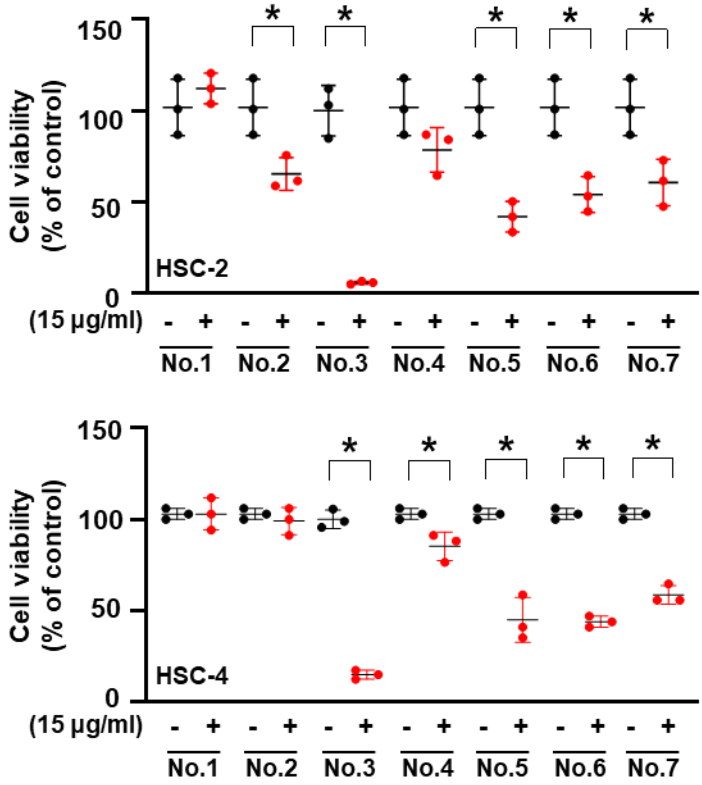

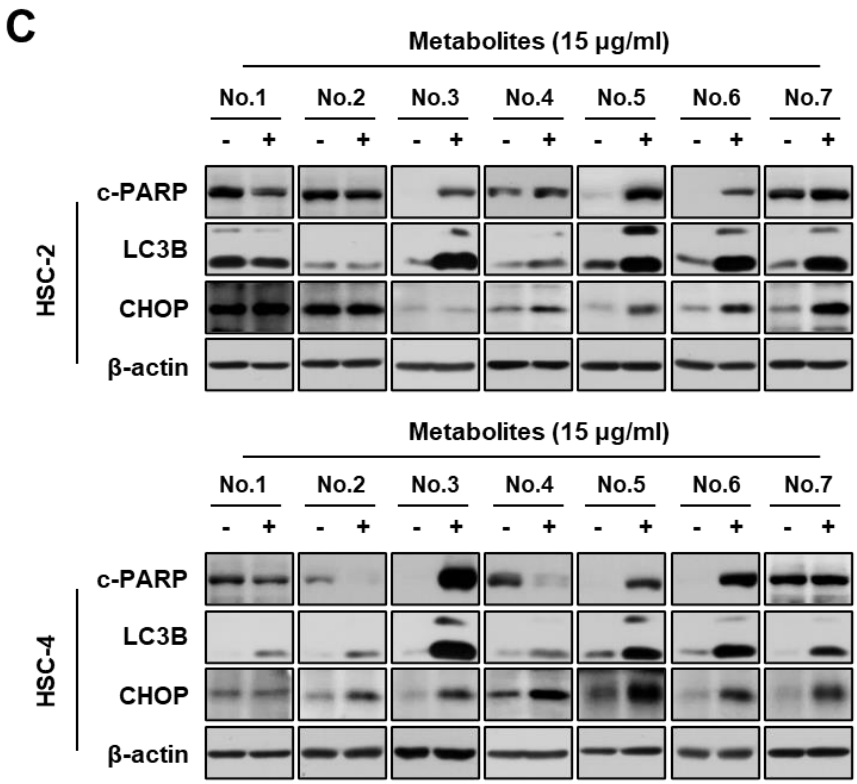

Fig. 10. Isolation and identification of ZOE components targeting CHOP protein is accompanied by autophagy and apoptosis.

(A) Representative HPLC chromatogram of ZO (70% ethanol extract) in the range of 20–80 min. Seven active components of ZO in the black line boxed area are listed to the right. AU indicates the absorbance unit. (B) Cell viability was assessed by trypan blue exclusion assay. All graphs represent the mean ± SD of three independent experiments. *, $P < 0.05$ by one-way ANOVA. (C)

Western blot images showing the expression levels of cleaved PARP, LC3-II, and CHOP in cells exposed to 15 μg/mL of the active components. β-actin was used as a loading control.

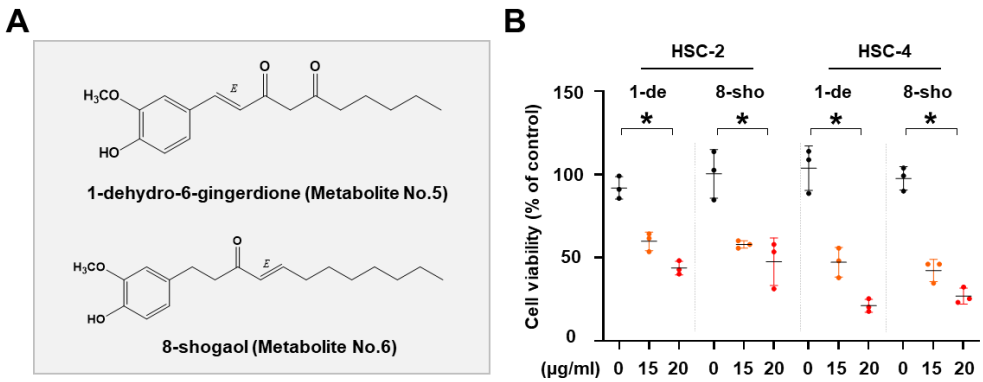

Fig. 11. The effects of 1-dehydro-6-gingerdione and 8-shogaol as active components of ZOE in human OSCC cell lines. HSC-2 and HSC-4 cells were treated with DMSO or the indicated concentrations of 1-dehydro-6-gingerdione or 8-shogaol for 24 h. **(A)** Chemical structures of 1-dehydro-6-gingerdione and 8-shogaol. **(B)** Cell viability was assessed by trypan blue exclusion assay. All graphs are the mean ± SD of three independent experiments. *, $P < 0.05$ by one-way ANOVA.

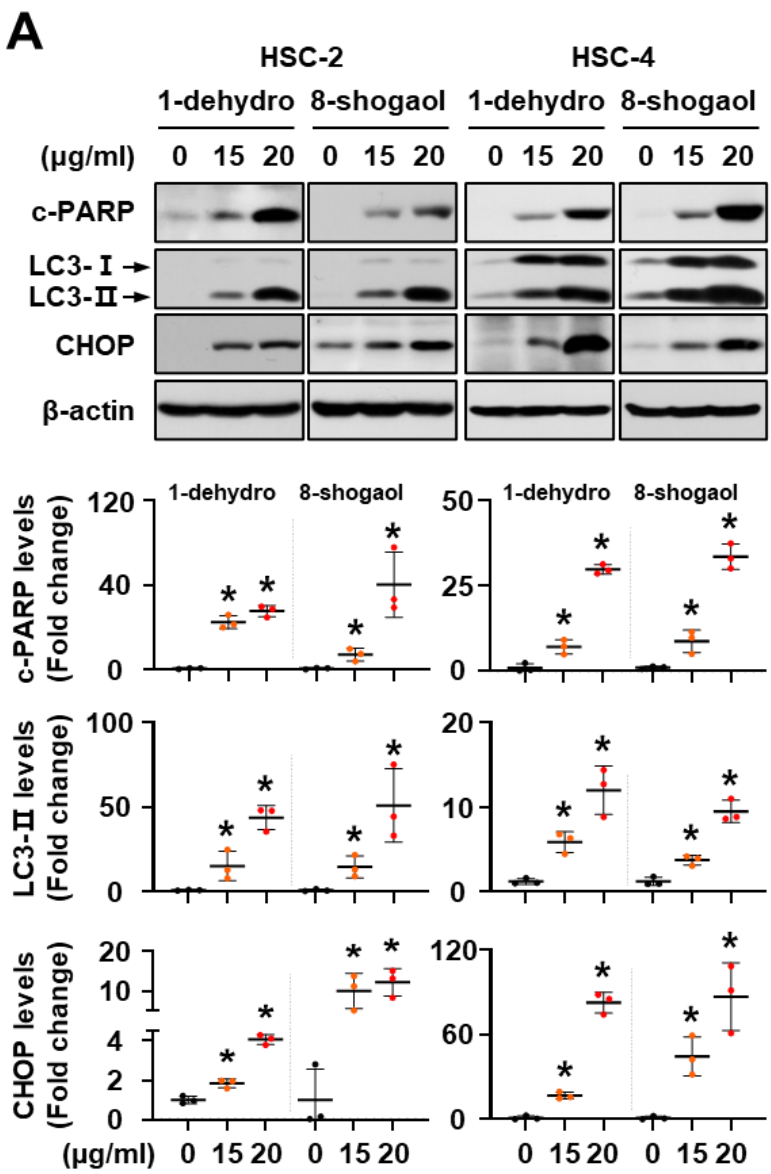
A
HSC-2
HSC-4
1-dehydro
8-shogaol
1-dehydro
8-shogaol
(μg/ml)
0 15 20 0 15 20 0 15 20 0 15 20
c-PARP
LC3- Ⅰ
LC3-Ⅱ
CHOP
β-actin
c-PARP levels (Fold change)
LC3-Ⅱ levels (Fold change)
CHOP levels (Fold change)
1-dehydro
8-shogaol
1-dehydro
8-shogaol
(μg/ml)
0 15 20 0 15 20 0 15 20 0 15 20

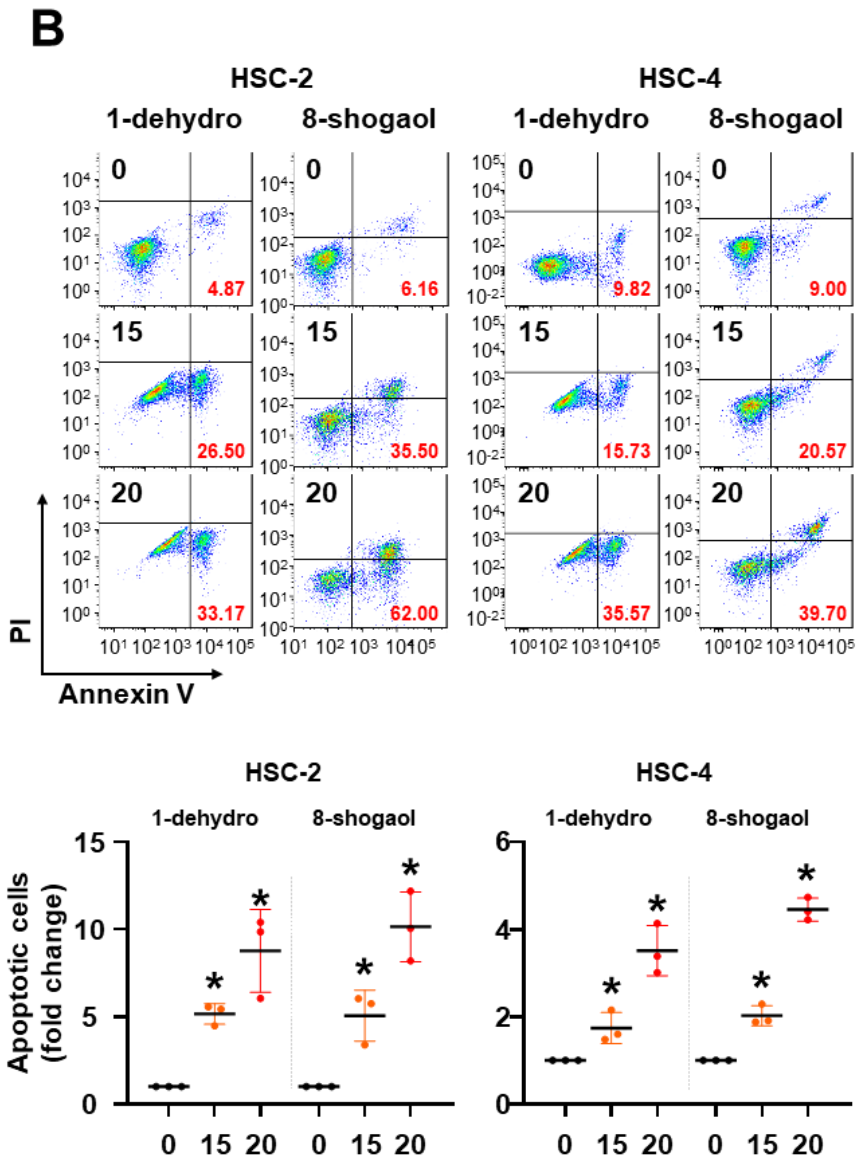

Fig. 12. The effects of 1-dehydro-6-gingerdione and 8-shogaol as active components of ZOE in human OSCC cell lines. HSC-2 and HSC-4 cells were treated with DMSO or the indicated concentrations of 1-dehydro-6-gingerdione or 8-shogaol for 24 h. (A) Western

blot images showing the expression levels of cleaved PARP, LC3-II, and CHOP in cells exposed to 1-dehydro-6-gingerdione and 8-shogaol. β-actin was used as a loading control. **(B)** Representative images of annexin V/PI double staining. All graphs are the mean ± SD of three independent experiments. *, $P < 0.05$ by one-way ANOVA or two-tailed Student's t-test.

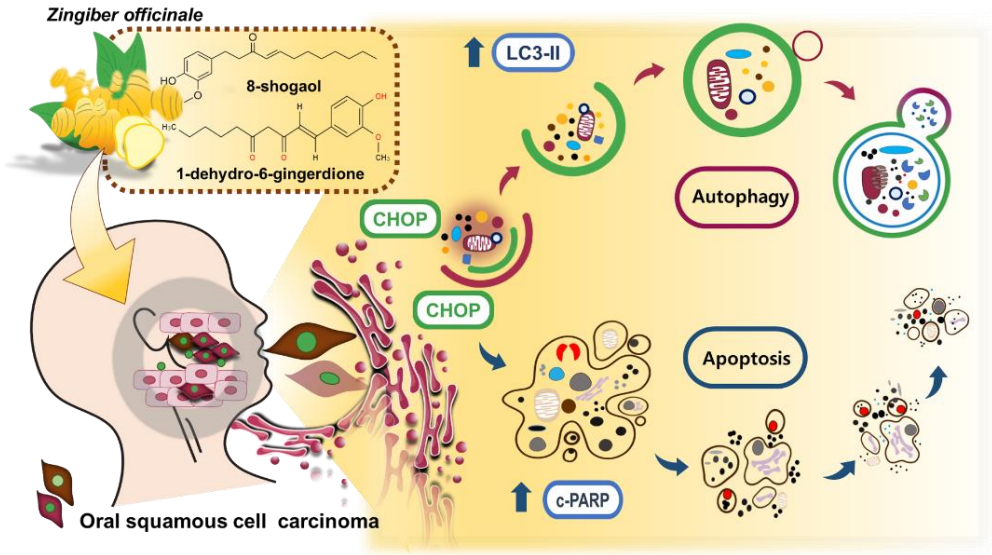

Fig. 13. Schematic illustration. ZOE shows anti-cancer activity in OSCC *in vitro* by inducing ER stress-mediated autophagy initiation and apoptosis, possibly through the effect of 1-dehydro-6-gingerdione and 8-shogaol, the two single active components.

4. Discussion

In this study, I evaluated ZOE as a potential anti-cancer drug candidate by measuring its cytotoxic activity against human OSCC *in vitro*. The mechanism by which ZOE suppresses the growth of OSCC cell lines was, in part, associated with the induction of ER stress-mediated autophagy initiation and apoptosis. Furthermore, 1-dehydro-6-gingerdione and 8-shogaol were identified as the main active components of ZOE and exhibited similar effects compared with that of ZOE against OSCC *in vitro*.

Autophagy is a very intricate mechanism consisting of dynamic and multistage processes including autophagosome formation, autophagosome-lysosome fusion (formation of autolysosomes), and cargo degradation (Glick et al, 2010). To understand the functional significance and underlying mechanism of autophagy more precisely, it is important to examine autophagic activity by measuring the degradation of cytoplasmic materials, known as autophagic flux (Mizushima and Murphy, 2020). In a cellular environment in which autophagy flux is induced, the cargo adaptor protein, p62, is relatively low in abundance because of its degradation by the lysosomal system

(Islam et al, 2018). However, in this study, I found that p62 was significantly increased in ZOE-treated cells, suggesting a blockage of autophagic flux induced by ZOE treatment in human OSCC cells. This was further supported by LC3-II accumulation in cells cotreated with CQ and ZOE and increased yellow puncta in ZOE-treated cells expressing the mCherry-GFP-LC3B plasmid. Autophagic flux can be inhibited by the downregulation of lysosomal membrane protein LAMP-2, responsible for autolysosome formation (Li et al, 2018). A recent study demonstrated that the blockage of autophagic flux in colorectal cancer cells was attributed to the inhibition of lysosomal acidification and lysosomal proteinase activity (Pan et al, 2019). In this study, I found that ZOE increased autophagosome and autolysosome formation in human OSCC cell lines using TEM analysis. This suggests that the reduced autophagic flux in human OSCC cells following ZOE treatment may be associated with the obstruction of lysosomal acidification rather than decreased maturation of autophagosomes into autolysosomes. Thus, I hypothesize that autophagosome accumulation following ZOE treatment may be the result of reduced autophagic flux, rather than

an antecedent event that enables the autophagy process.

The ER is the salient organelle responsible for proper protein folding, modification, and maturation and is a reservoir of intracellular calcium (Hetz, 2012). If ER function is disrupted by various stimuli, cells experience an accumulation of unfolded or misfolded proteins in the ER lumen, resulting in ER stress and the activation of the unfolded protein response to restore ER homeostasis. Nonetheless, if cells are constantly exposed to prolonged ER stress or fail to restore ER homeostasis, cell death mechanisms are triggered (Hetz, 2012). Exposure to various cancer therapeutics results in ER stress, which contributes to the induction of apoptosis and/or autophagy (Chen et al, 2018, Rubiolo et al, 2014, Zhang et al, 2019). CHOP is a key regulator during ER stress and is responsible for ER stress-mediated autophagy and apoptosis (Kim et al, 2018, Ma et al, 2020). The accumulation of CHOP is sufficient to induce autophagic apoptosis as evidenced by a decrease and sequestration of the antiapoptotic protein, Bcl-2, and the release of Beclin1, an essential protein for autophagosome formation (Liu et al, 2014). Thus, ER stress has an important regulatory role in cellular events, such as

autophagy and/or apoptosis. In this study, ZOE significantly increased the expression of CHOP in a dose- and time-dependent manner, which simultaneously may facilitate autophagy initiation and apoptosis induction. Therefore, the simultaneous induction of autophagy initiation and apoptosis by ZOE may be the result of the upregulation of CHOP during ER stress.

5. Conclusion

In this study, I demonstrated that ZOE exhibits anti-cancer activity in OSCC *in vitro* by facilitating ER stress-mediated autophagy initiation and apoptosis, possibly through the action of 1-dehydro-6-gingerdione and 8-shogaol, the two single active components. Therefore, ZOE and its two active components may be useful anti-cancer drug candidates with therapeutic potential against human OSCC (Fig. 13).

6. References

ABDULLAH, S., ABIDIN, S. A. Z., MURAD, N. A., MAKPOL, S., NGAH, W. Z. W. & YUSOF, Y. A. M. Ginger extract (*Zingiber officinale*) triggers apoptosis and G0/G1 cells arrest in HCT 116 and HT 29 colon cancer cell lines. *African Journal of Biochemistry Research*. 2010;4(5):134-142.

ANSARI, J. A., AHMAD, M. K., KHAN, A. R., FATIMA, N., KHAN, H. J., RASTOGI, N., MISHRA, D. P. & MAHDI, A. A. Anticancer and Antioxidant activity of *Zingiber officinale* Roscoe rhizome. *Indian Journal of Experimental Biology*. Nov 2016;54(11):767-773.

BAI, L. & WANG, S. Targeting apoptosis pathways for new cancer therapeutics. *Annual Review of Medicine*. 2014;65:139-155. doi:10.1146/annurev-med-010713-141310

CHAMBERLIN, S. R., BLUCHER, A., WU, G., SHINTO, L., CHOONOO, G., KULESZ-MARTIN, M. & MCWEENEY, S. Natural Product Target Network Reveals Potential for Cancer Combination Therapies. *Frontiers in Pharmacology*. 2019;10:557. doi:10.3389/fphar.2019.00557

CHEN, W., LI, P., LIU, Y., YANG, Y., YE, X., ZHANG, F. & HUANG, H. Isoalantolactone induces apoptosis through ROS-mediated ER stress and inhibition of STAT3 in prostate cancer cells. *Journal of Experimental and Clinical Cancer Research*. 2018;37(1):1-12.

ELKADY, A. I., ABUZINADAH, O. A., BAESHEN, N. A. & RAHMY, T. R. Differential control of growth, apoptotic activity, and gene expression in human breast cancer cells by extracts derived from

medicinal herbs *Zingiber officinale*. *Journal of Biomedicine & Biotechnology*. 2012;2012:614356. doi:10.1155/2012/614356

FERNALD, K. & KUROKAWA, M. Evading apoptosis in cancer. *Trends in Cell Biology*. Dec 2013;23(12):620-633. doi:10.1016/j.tcb.2013.07.006

GLICK, D., BARTH, S. & MACLEOD, K. F. Autophagy: cellular and molecular mechanisms. *Journal of Pathology*. May 2010;221(1):3-12. doi:10.1002/path.2697

HETZ, C. The unfolded protein response: controlling cell fate decisions under ER stress and beyond. *Nature Reviews: Molecular Cell Biology*. Jan 18 2012;13(2):89-102. doi:10.1038/nrm3270

ISLAM, M. A., SOORO, M. A. & ZHANG, P. Autophagic Regulation of p62 is Critical for Cancer Therapy. *International Journal of Molecular Sciences*. May 8 2018;19(5)doi:10.3390/ijms19051405

KIM, T. W., LEE, S. Y., KIM, M., CHEON, C. & KO, S. G. Kaempferol induces autophagic cell death via IRE1-JNK-CHOP pathway and inhibition of G9a in gastric cancer cells. *Cell Death & Disease*. Aug 29 2018;9(9):875. doi:10.1038/s41419-018-0930-1

LEE, S. W., LIM, J.-H., KIM, M. S., JEONG, J.-H., SONG, G.-Y., LEE, W. S. & RHO, M.-C. Phenolic compounds isolated from *Zingiber officinale* roots inhibit cell adhesion. *Food Chemistry*. 2011;128(3):778-782.

LI, Z., ZHU, S., HUANG, L., SHANG, M., YU, C., ZHU, H., HAN, D., HUANG, H., YU, X. & LI, X. Exendin-4 impairs the autophagic flux to induce apoptosis in pancreatic acinar AR42J cells by down-regulating LAMP-2. *Biochemical and Biophysical Research Communications*. Feb 5 2018;496(2):294-301. doi:10.1016/j.bbrc.2018.01.037

LING, H., YANG, H., TAN, S. H., CHUI, W. K. & CHEW, E. H. 6-Shogaol, an active constituent of ginger, inhibits breast cancer cell invasion by reducing matrix metalloproteinase-9 expression via blockade of nuclear factor-kappaB activation. *British Journal of Pharmacology*. Dec 2010;161(8):1763-1777. doi:10.1111/j.1476-5381.2010.00991.x

LIU, K., SHI, Y., GUO, X., WANG, S., OUYANG, Y., HAO, M., LIU, D., QIAO, L., LI, N., ZHENG, J. & CHEN, D. CHOP mediates ASPP2-induced autophagic apoptosis in hepatoma cells by releasing Beclin-1 from Bcl-2 and inducing nuclear translocation of Bcl-2. *Cell Death & Disease*. Jul 17 2014;5:e1323. doi:10.1038/cddis.2014.276

MA, Y. Y., DI, Z. M., CAO, Q., XU, W. S., BI, S. X., YU, J. S., SHEN, Y. J., YU, Y. Q., SHEN, Y. X. & FENG, L. J. Xanthatin induces glioma cell apoptosis and inhibits tumor growth via activating endoplasmic reticulum stress-dependent CHOP pathway. *Acta Pharmacologica Sinica*. Mar 2020;41(3):404-414. doi:10.1038/s41401-019-0318-5

MANSINGH, D. P., OJ, S., SALI, V. K. & VASANTHI, H. R. [6]-Gingerol-induced cell cycle arrest, reactive oxygen species generation, and disruption of mitochondrial membrane potential are associated with apoptosis in human gastric cancer (AGS) cells. *Journal of Biochemical and Molecular Toxicology*. 2018;32(10):e22206.

MIZUSHIMA, N. & MURPHY, L. O. Autophagy Assays for Biological Discovery and Therapeutic Development. *Trends in Biochemical Sciences*. Dec 2020;45(12):1080-1093. doi:10.1016/j.tibs.2020.07.006

NIKKHAH BODAGH, M., MALEKI, I. & HEKMATDOOST, A. Ginger in gastrointestinal disorders: A systematic review of clinical trials. *Food Sci Nutr*. Jan 2019;7(1):96-108. doi:10.1002/fsn3.807

PAN, H., WANG, Y., NA, K., WANG, Y., WANG, L., LI, Z., GUO, C., GUO, D. & WANG, X. Autophagic flux disruption contributes to Ganoderma lucidum polysaccharide-induced apoptosis in human colorectal cancer cells via MAPK/ERK activation. *Cell Death & Disease*. Jun 11 2019;10(6):456. doi:10.1038/s41419-019-1653-7

RADHAKRISHNAN, E. K., BAVA, S. V., NARAYANAN, S. S., NATH, L. R., THULASIDASAN, A. K., SONIYA, E. V. & ANTO, R. J. [6]-Gingerol induces caspase-dependent apoptosis and prevents PMA-induced proliferation in colon cancer cells by inhibiting MAPK/AP-1 signaling. *PloS One*. 2014;9(8):e104401. doi:10.1371/journal.pone.0104401

RAHMANI, A. H. Active ingredients of ginger as potential candidates in the prevention and treatment of diseases via modulation of biological activities. *International Journal of Physiology, Pathophysiology and Pharmacology*. 2014;6(2):125.

RUBIOLO, J. A., LOPEZ-ALONSO, H., MARTINEZ, P., MILLAN, A., CAGIDE, E., VIEYTES, M. R., VEGA, F. V. & BOTANA, L. M. Yessotoxin induces ER-stress followed by autophagic cell death in glioma cells mediated by mTOR and BNIP3. *Cellular Signalling*. Feb 2014;26(2):419-432.

SAHA, A., BLANDO, J., SILVER, E., BELTRAN, L., SESSLER, J. & DIGIOVANNI, J. 6-Shogaol from dried ginger inhibits growth of prostate cancer cells both *in vitro* and in vivo through inhibition of STAT3 and NF-κB signaling. *Cancer prevention research*. 2014;7(6):627-638.

SHI, S., TAN, P., YAN, B., GAO, R., ZHAO, J., WANG, J., GUO, J., LI, N. & MA, Z. ER stress and autophagy are involved in the apoptosis induced by cisplatin in human lung cancer cells. *Oncology Reports*. May 2016;35(5):2606–2614. doi:10.3892/or.2016.4680

SONG, S., TAN, J., MIAO, Y., LI, M. & ZHANG, Q. Crosstalk of autophagy and apoptosis: Involvement of the dual role of autophagy under ER stress. *Journal of Cellular Physiology*. Nov 2017;232(11):2977–2984. doi:10.1002/jcp.25785

YANG, Y. & KLIONSKY, D. J. Autophagy and disease: unanswered questions. *Cell Death and Differentiation*. Mar 2020;27(3):858–871. doi:10.1038/s41418–019–0480–9

YONEKAWA, T. & THORBURN, A. Autophagy and cell death. *Essays in Biochemistry*. 2013;55:105–117. doi:10.1042/bse0550105

ZHANG, X., HU, P., DING, S.–Y., SUN, T., LIU, L., HAN, S., DELEO, A. B., SADAGOPAN, A., GUO, W. & WANG, X. Induction of autophagy–dependent apoptosis in cancer cells through activation of ER stress: an uncovered anti–cancer mechanism by anti–alcoholism drug disulfiram. *American Journal of Cancer Research*. 2019;9(6):1266.

ZHOU, F., LI, Y. H., WANG, J. J., PAN, J. & LU, H. Endoplasmic reticulum stress could induce autophagy and apoptosis and enhance chemotherapy sensitivity in human esophageal cancer EC9706 cells by mediating PI3K/Akt/mTOR signaling pathway. *Tumour Biology*. Jun 2017;39(6):1010428317705748. doi:10.1177/1010428317705748

국문 초록

구강 편평상피세포암종에서 C/EBP Homologous protein을 통한 자가포식과 세포사멸을 유도하는 생강추출물 및 생리활성물질의 항암 효능에 관한 연구

김 현 지

서울대학교 대학원

치의과학과 구강병리학 전공

지도 교수: 조 성 대

1. 목적: 생강추출물 및 주요 생리활성물질은 여러 암종에서 다양한 매커니즘을 통해 항암 효능을 보이는 것으로 알려져 있다. 하지만 구강 편평상피세포암종에서 이들의 항암 효능에 대한 연구는 현재까지 미미한 실정이다. 따라서, 본 연구에서는 구강 편평상피세포암종 세포주에서 자가포식 (autophagy) 및 세포사멸 (apoptosis)을 유도하는 생강추출물과 주요 생리활성물질인 1-dehydro-6-gingerdione 및 8-shogaol의 항암 효능에 대해 조사하였다.

2. 재료 및 방법: 구강 편평상피세포암종에서 생강추출물 및 생리활성물질의 세포사멸에 대한 효능은 cleaved PARP 단백질의 검출, DAPI 염색, sub-G1 분석 또는 Annexin V/PI double staining을 통해 평가되었다. 생강추출물 및 생리활성물질의 자가포식에 대한 효능은 LC3-Ⅱ 단백질의 검출, 투과전자현미경 관찰, acidic vesicular organelle 또는 LC3 puncta 형성을 관찰함으로써 평가되었다. 또한, 생강추출물의 자가포식 유동 (autophagic flux)에 대한 효능은 자가포식 억제제인 클로로퀸 (Chloroquine)을 병용투여 한 후, LC3-Ⅱ 단백질 검출, LC3 puncta 형성 및 mCherry-GFP-LC3 형광벡터를 사용함으로써 증명되었다. 소포체 스트레스 (ER stress)는 C/EBP Homologous protein (CHOP)의 검출을 통해 확인되었다. 생강추출물의 생리활성물질은 gas chromatography/mass spectrometry (GC/MS)를 통해 확인 및 분리되었다.

3. 결과 및 고찰: 생강추출물과 주요 생리활성물질인 1-dehydro-6-gingerdione 및 8-shogaol은 구강 편평상피세포암종 세포주에서 세포증식을 억제하였다. 생강추출물은 cleaved PARP 단백질의 발현을 증가시키고, 핵 응축과 DNA 분절을 유도, sub-G1 population 및 Annexin V-stained population을 증가시키는 것을 통해서 세포사멸이 유도되었음을 확인하였다. 또한 생강추출물은 LC3-II 단백질의 발현을

증가시킬 뿐만 아니라, 이중 막 구조를 가진 자가식포(autophagosome)의 형성, acidic vesicular organelle 및 LC3 puncta 형성을 증가시킴으로써 자가포식을 유도하였으며, 이는 자가포식 유동 억제가 관련되어 있음을 확인하였다. 구강 편평상피세포암종에서 생강추출물의 자가포식 및 세포사멸에 대한 효능은 소포체 스트레스 관련 단백질인 CHOP의 증가를 통해 초래됨을 확인하였다. Gas chromatography/mass spectrometry를 통해 생강추출물의 주요 생리활성물질인 1-dehydro-6-gingerdione 및 8-shogoal을 분리하였고, 이 주요 생리활성물질이 CHOP의 발현을 증가시킴으로써 자가포식 및 세포사멸을 유도할 수 있는 생강추출물의 항암 효능에 기여하는 유효 성분일 가능성이 있음을 확인하였다.

주요어: *Zingiber officinale*; Oral squamous cell carcinoma; Apoptosis; Autophagy; 1-dehydro-6-gingerdione; 8-shogaol

학번: 2020-27195